

pubs.acs.org/JACS Article

Proteomimetic Polymers Trigger Potent Antigen-Specific T Cell Responses to Limit Tumor Growth

Max M. Wang, Mi-Ran Choi, Claudia Battistella, Brayley Gattis, Baofu Qiao, Michael Evangelopoulos, Chad A. Mirkin, Monica Olvera de la Cruz, Bin Zhang, and Nathan C. Gianneschi



Cite This: J. Am. Chem. Soc. 2024, 146, 14959-14971



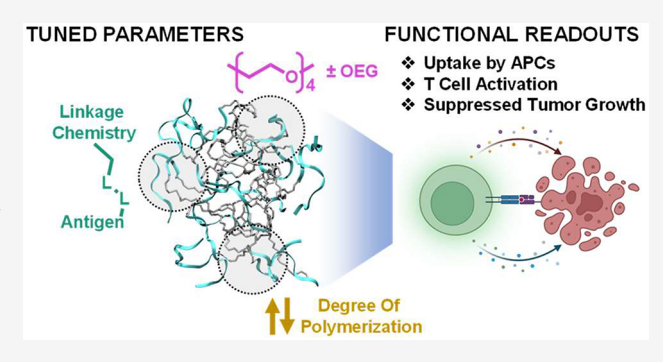
ACCESS

III Metrics & More

Article Recommendations

s Supporting Information

ABSTRACT: Elicitation of effective antitumor immunity following cancer vaccination requires the selective activation of distinct effector cell populations and pathways. Here we report a therapeutic approach for generating potent T cell responses using a modular vaccination platform technology capable of inducing directed immune activation, termed the Protein-like Polymer (PLP). PLPs demonstrate increased proteolytic resistance, high uptake by antigen-presenting cells (APCs), and enhanced payload-specific T cell responses. Key design parameters, namely payload linkage chemistry, degree of polymerization, and side chain composition, were varied to optimize vaccine formulations. Linking antigens to the polymer backbone using an intracellularly cleaved disulfide bond



copolymerized with a diluent amount of oligo(ethylene glycol) (OEG) resulted in the highest payload-specific potentiation of antigen immunogenicity, enhancing dendritic cell (DC) activation and antigen-specific T cell responses. Vaccination with PLPs carrying either gp100, E7, or adpgk peptides significantly increased the survival of mice inoculated with B16F10, TC-1, or MC38 tumors, respectively, without the need for adjuvants. B16F10-bearing mice immunized with gp100-carrying PLPs showed increased antitumor CD8⁺ T cell immunity, suppressed tumor growth, and treatment synergy when paired with two distinct stimulator of interferon gene (STING) agonists. In a human papillomavirus-associated TC-1 model, combination therapy with PLP and 2'3'-cGAMP resulted in 40% of mice completely eliminating implanted tumors while also displaying curative protection from rechallenge, consistent with conferment of lasting immunological memory. Finally, PLPs can be stored long-term in a lyophilized state and are highly tunable, underscoring the unique properties of the platform for use as generalizable cancer vaccines.

■ INTRODUCTION

Cancer immunotherapy, which utilize the immune system to eradicate tumors, is a promising therapeutic approach for generating personalized treatments. Clinically successful examples include immune checkpoint inhibitors, chimeric antigen receptor T (CAR-T) cell therapy, and therapeutic cancer vaccines. Cancer vaccine development in particular has taken advantage of innovations in nanocarrier technologies to improve efficacy by selective trafficking to lymphoid organs and codelivery of antigens with adjuvants. 4-7 Since elicitation of antigen-specific immune responses following vaccination requires the recruitment of multiple immune cell populations and orchestration of complex signaling pathways, generating durable therapies has remained a challenge. Major barriers preventing vaccine induced antitumor immunity include poor immunogenicity of tumor-associated antigens and limited spatiotemporal control over antigen cross-presentation and production of costimulatory signals required for T cell priming.³ To circumvent these limitations, cancer vaccines using neoantigens have been employed with promising early phase clinical trial results.^{8–10} However, several significant hurdles remain to be addressed. First, peptide epitopes are susceptible to rapid proteolytic cleavage, dampening the raised immune reaction. Second, the efficient delivery of vaccine components to professional antigen-presenting cells (APCs) residing in secondary lymphoid organs has remained challenging. Third, available technologies are inefficient at codelivering multiple heterologous epitope antigens with adjuvants to raise broad spectrum immune responses. Therefore, there is an unmet clinical need for platform technologies capable of potentiating neoantigen immunogenicity to propagate durable cancer immunotherapies.

We report here the development of a cancer vaccine approach built on a modular peptide brush polymer platform technology termed the Protein-like Polymer (PLP), in

Received: May 23, 2023 Revised: August 21, 2023 Accepted: August 22, 2023 Published: May 23, 2024





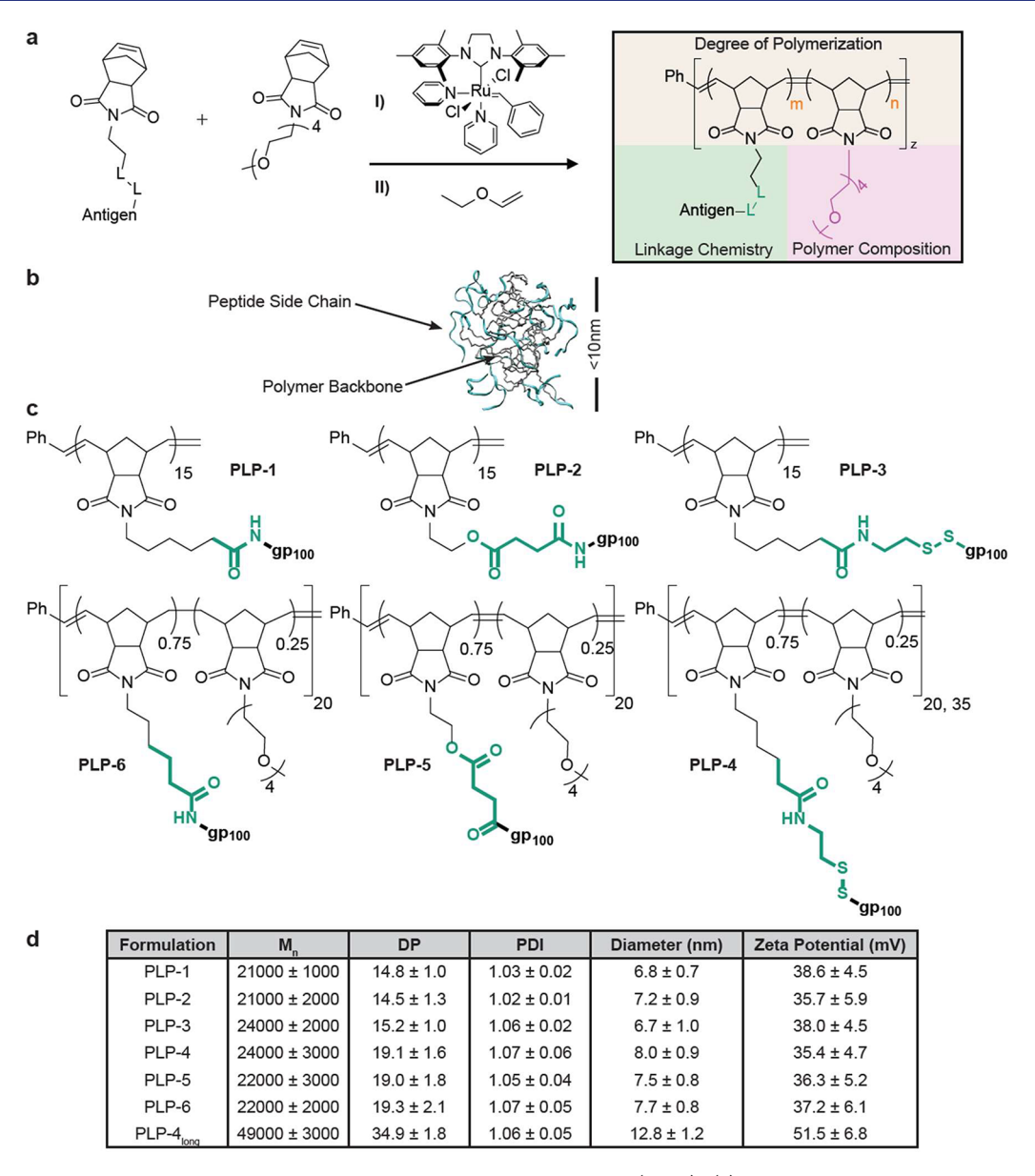


Figure 1. Synthesis and characterization of immunostimulatory Protein-like Polymers (PLPs). (a) Synthetic scheme showing gene ration of PLPs from norbornenyl-peptide monomers via ROMP and summary schematic of physical parameters optimized. L-L: linkage chemistry. (b) Representative *in silico* model of a generalized PLP (DP: 15) in aqueous solution. (c) Three distinct linker chemistries (green) were used to construct antigen-PLP conjugates: Amide (PLP-1, -6), Ester (PLP-2, -5), and Disulfide (PLP-3, -4). Blended copolymers of each linker were made with the OEG interdigitated throughout. Theoretical DPs labeled—see Table S4 for experimental batch characterization. (d) Characterization of PLPs, including number-average molecular weight (M_n), degree of polymerization (DP), and dispersity (PDI) as determined by SEC-MALS, as well as hydrodynamic diameter in H₂O measured by DLS and surface charge (n = 3-4 separate syntheses).

reference to its globular three-dimensional structure consisting of peptide side chains covalently linked to and wrapped around a hydrophobic polymeric core. PLP architectures can be rapidly optimized for desired functionalities by controlling side-chain peptide identity, linkage and backbone chemistry, and molecular weight. Compared to current nanotechnologies employed for cancer vaccines (e.g., nanoparticles, nanodiscs, scaffolds, microparticles, etc.), the PLP platform allows for much higher levels of control over peptide incorporation, as they are attached covalently forming single polymer chains not reliant on self-assembly into noncovalent nanoscale materials, and storable long-term in a lyophilized state. PLPs are generated using two robust chemical processes: (1) solid-support synthesis of desired native peptide sequences

containing a polymerizable functional group requiring minimal chemical modification of the payload and (2) living polymerization of peptide monomers yielding densely arrayed peptide brushes with narrow polydispersity where every side chain is a predetermined amino acid sequence (Figure 1a,b). PLPs employed in this work were synthesized via ring-opening metathesis polymerization (ROMP), allowing for control of side chain incorporation and degree of polymerization (DP) through modulating the order of monomer addition and monomer to initiator ratios, respectively. ^{12,13}

To ascertain design rules for immunostimulatory PLPs, three key parameters were modulated: (*i*) antigen linkage chemistry; (*ii*) incorporation of oligo(ethylene glycol) (OEG); and (*iii*) DP (Figure 1a). PLPs were found to be more efficient at

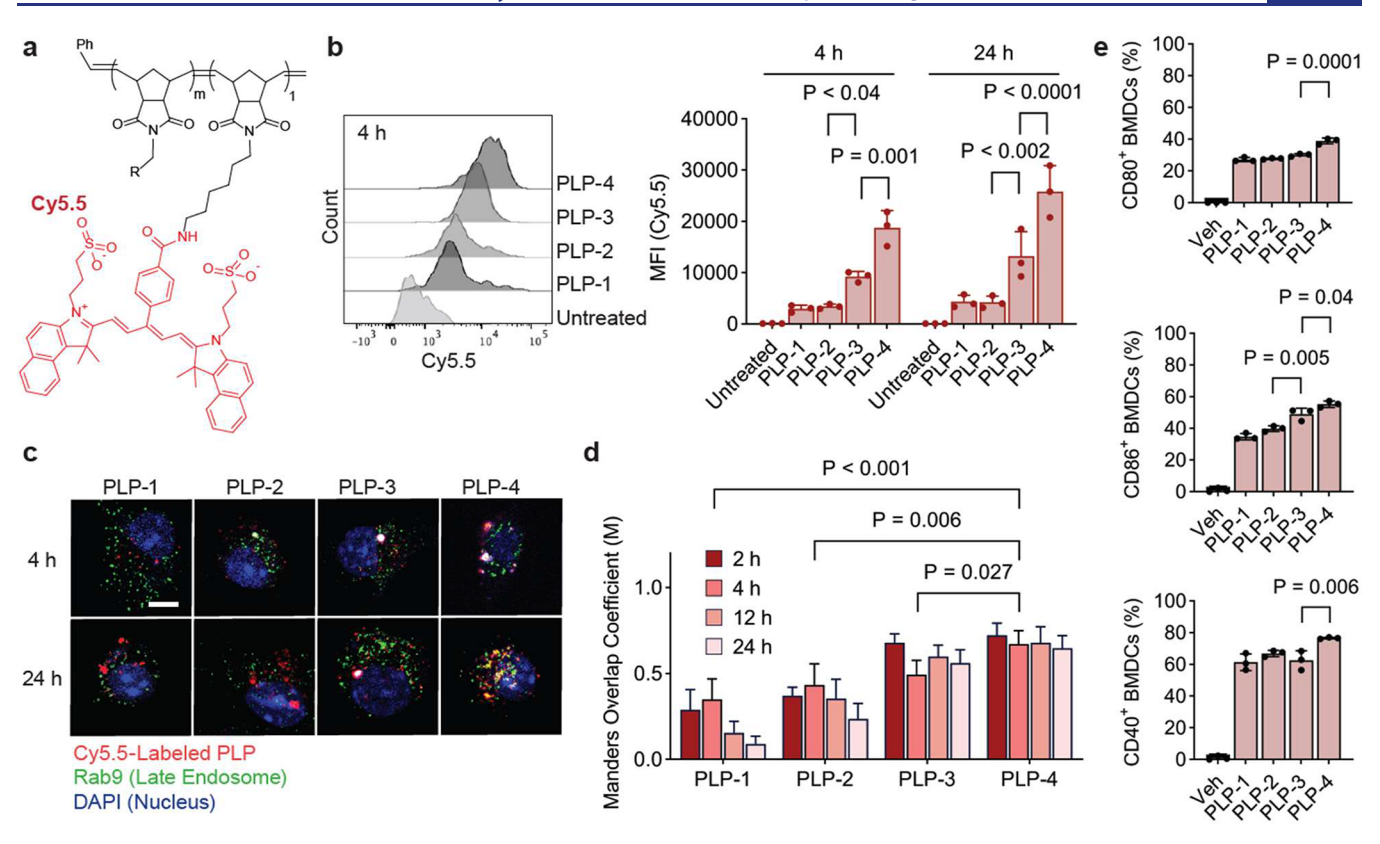


Figure 2. Uptake and trafficking profiles of PLPs over time. (a) Cy5.5-labeled versions of PLP-1, 2, 3, and 4 were made by copolymerizing 1 equiv of dye-monomer added at the end of the reaction. Cy5.5 structure shown in red. (b) Uptake of PLPs by splenic DCs following 4 or 24 h incubation, measured by flow cytometry. Representative histogram shown. MFI: Median Fluorescence Intensity. (c) Representative confocal images of labeled PLPs (Cy5.5, red) and late endosomes (Alexa-488, green, Rab9) following 4 or 24 h incubation with BMDCs. Scale bar: 5 μm. (d) Manders overlap coefficient (M) quantifying fraction of Cy5.5 signal colocalized with Rab9. M > 0.6 indicates strong colocalization (n = 10-15 randomly selected images per group, two independent experiments). PLPs were dosed at 0.5 μM of Cy5.5. (e) Expression of CD80, CD86, or CD40 in BMDCs following 24 h incubation with indicated PLPs. Data depict mean \pm s.d. P-values determined using one- (b,e) or two-way (c, 4 h values shown) ANOVAs.

eliciting a payload-specific immune response compared to liposomes containing the same tumor antigen. Importantly, PLPs can be stored long-term in a lyophilized state with minimal loss of activity, a comparative advantage over alternative technologies. Furthermore, PLP vaccination triggered potent and durable antitumor immunity in three different tumor models, which synergized with two different agonists of stimulator of interferon genes (STING). We present here the first successful demonstration of the PLP platform technology as a cancer vaccine capable of eliciting payload-specific immune activation, resulting in reductions in disease burden and establishing a paradigm for constructing polymer-based vaccine candidates with superior clinical utility.

RESULTS

Design and Characterization of PLPs with Different Linkages. $gp100_{25-33}$, a MHC class I restricted tumorassociated antigen expressed in melanocytes, was first used as a proof-of-concept model system due to its ability to elicit specific cytotoxic T lymphocyte (CTL) mediated immune responses leading to regression of established B16F10 melanoma. Three classes of PLPs were designed where human melanoma-specific antigenic peptide, gp100 (KVPRNQDWL), was attached to the polymer backbone using three linkage chemistries: a noncleavable amide, an easily hydrolyzed ester, and an intracellularly cleavable disulfide

(Figure 1c). We used an approximately six-carbon linker between the first amino acid and the norbornene unit, which has previously been shown to polymerize rapidly with high percent conversion¹⁷ (Figure S1). Ester bonds are indiscriminately cleaved by esterases, ¹⁸ while APCs are known to reduce disulfide bonds as part of the antigen processing pathway, 19 a phenomenon that has been previously exploited in nano-particle formulations. ^{20–23} Monomers were prepared by coupling norbornenes functionalized with a carboxylic acid, hydroxyl, or pyridyldithio group to the N-terminus of the corresponding end-functionalized peptide sequence (Figure S1 and Table S1). Pyridyl disulfide chemistry was chosen due to its ease of synthesis and amenability to ROMP compared to other modifications, which fail to polymerize (i.e., unprotected cysteines¹⁷). ¹H NMR showed full consumption of the monomer and the appearance of resonances corresponding to the *cis* and *trans* olefinic protons of the polymer backbone after 8 h (Figure S2). PLPs were characterized by sizeexclusion chromatography with multiangle light scattering (SEC-MALS) to ascertain DP and molecular weight distribution, which agreed with apparent molecular weights, as determined by SDS-PAGE (Figure S3). Repeat polymerizations exhibited agreement between measured and theoretical DP based on initial monomer-to-initiator ratios ([M]₀/ $[I]_0$) with low dispersity $(M_w/M_n < 1.1)$ (Table S2). DPs within 10% of the desired value were considered to be

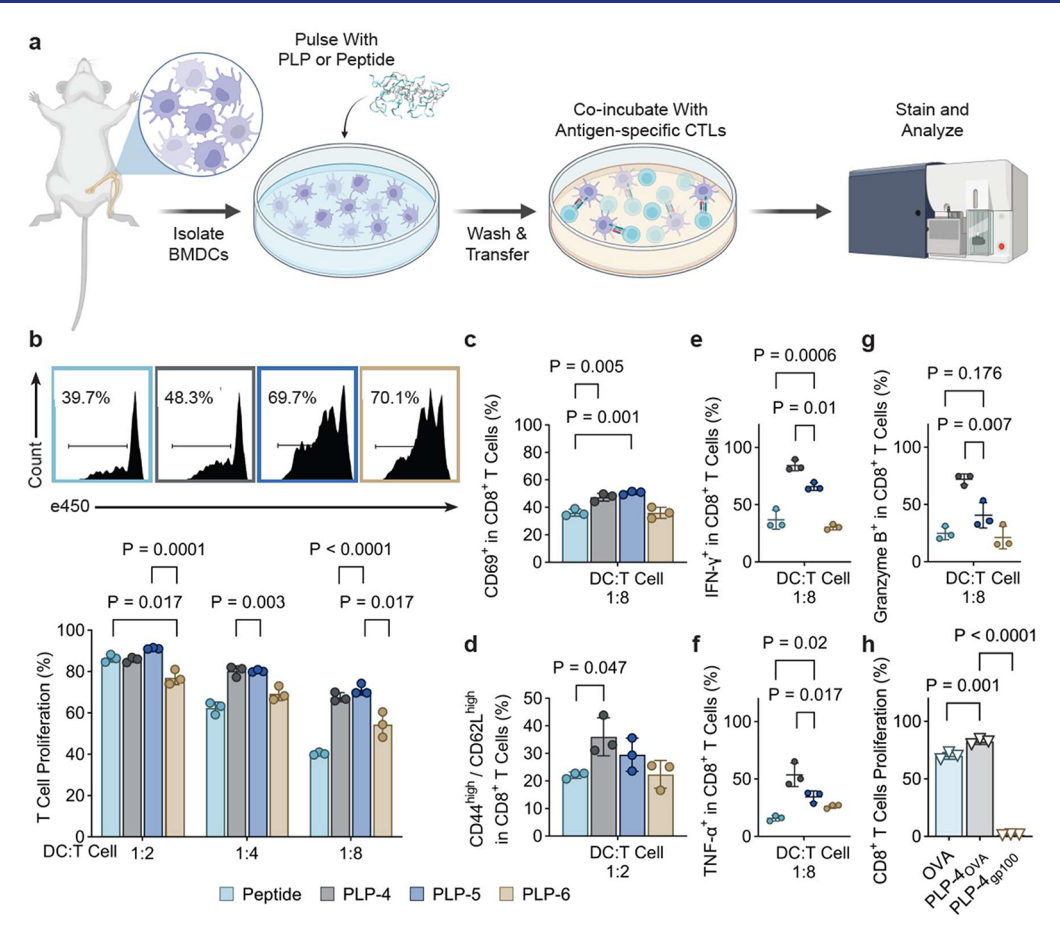


Figure 3. PLP pulsed DCs induce conjugation chemistry-dependent antigen-specific T cell responses. (a) Isolated CD11c⁺ BMDCs were pulsed with indicated treatments at 10 μ g/mL peptide concentration for 4 h, washed, and then cocultured with pmel CD8⁺ T cells at indicated ratios for 72 h. Created with BioRender.com. (b) CD8⁺ T cell proliferation measured by flow cytometry (n = 3 independent samples per group). Percentages of CD8⁺ T cells positive for CD69 (c) and expressed CD44^{high}/CD62L^{high} (d). Cytokine expression of IFN- γ (e), TNF- α (f), or Granzyme B (g) in CD8⁺ T cells analyzed using flow cytometry (n = 3 independent samples per group). (h) Proliferation of OT-1 CD8⁺ T cells following treatment with the OVA peptide (SIINFEKL), PLP-4_{OVA}, or PLP-4_{gp100} (n = 3 independent samples per group). Data depict mean \pm s.d. P-values determined by two (b) or one-way (c-h) ANOVA. Experiment repeated with similar results.

equivalent formulations. (See Table S4 for batch characterization).

Comparison of size and surface charge, known to play determining roles in cellular uptake and pharmacokinetic profiles, ^{24,25} showed no significant differences between linkage chemistries (Figure 1d, Figure S4). Previous studies on similar PLP structures have shown, by small-angle X-ray scattering (SAXS), that they resemble globular proteins morphologically, 26 a feature recapitulated by gp100-conjugated PLPs (Figure S5). To confirm antigen-PLP conjugates are reduction sensitive in a linkage-dependent manner, PLPs were incubated in PBS containing either 0 mM or 10 mM glutathione (GSH, physiologically relevant cytosolic concentration^{27,28}) with antigen release tracked by HPLC. As expected, >95% of the peptide antigen was released from PLP-3 after 24 h incubation in 10 mM GSH, whereas negligible peptide signal was detected in the absence of GSH. Conversely, no changes in antigen release were observed for PLP-1 and PLP-2 following GSH treatment (Figure S6). PLP-2 showed a minor antigen release independent of GSH, which is attributed to hydrolysis (Figure

PLPs Are Resistant to Enzymatic Degradation while Sustaining DC Activation. Incubation in supraphysiological concentrations (20× human serum levels²⁹) of model enzyme

trypsin was performed with cleavage monitored by HPLC. Free peptide was rapidly cleaved, whereas all PLP formulations had marked resistance to proteolysis. PLP-2 showed slightly higher rates of cleavage compared to PLP-1 and PLP-3 which can be attributed to the more labile nature of the ester bond (Figure S8a). Next, the ability of PLPs to activate bonemarrow derived dendritic cells (BMDCs) in vitro was assessed due to the cell type's potency as APCs and ability to elicit antitumor immunity when pulsed with tumor epitopes.³⁰⁻³² PLPs were incubated in mouse serum prior to treatment with BMDCs to mimic biological conditions. In the absence of serum pretreatment, CD86 expression in BMDCs was similar between PLP formulations and the free peptide. However, following overnight serum incubation, free peptide treatment showed significantly decreased CD86 levels compared to PLP treatments, which maintained BMDC activation (Figure S9). These results show that PLPs can resist enzymatic degradation, thereby sustaining APC activation under biological conditions.

Uptake and Trafficking of PLPs by DCs. Cellular uptake and intracellular localization of PLPs were assessed by incorporating a Cy5.5 fluorescent monomer on the polymer backbone (Figure 2a, see Supplemental Methods). A Cy5.5 standard curve was used to quantify dye incorporation and ensure similar fluorescence doses between groups (Figure

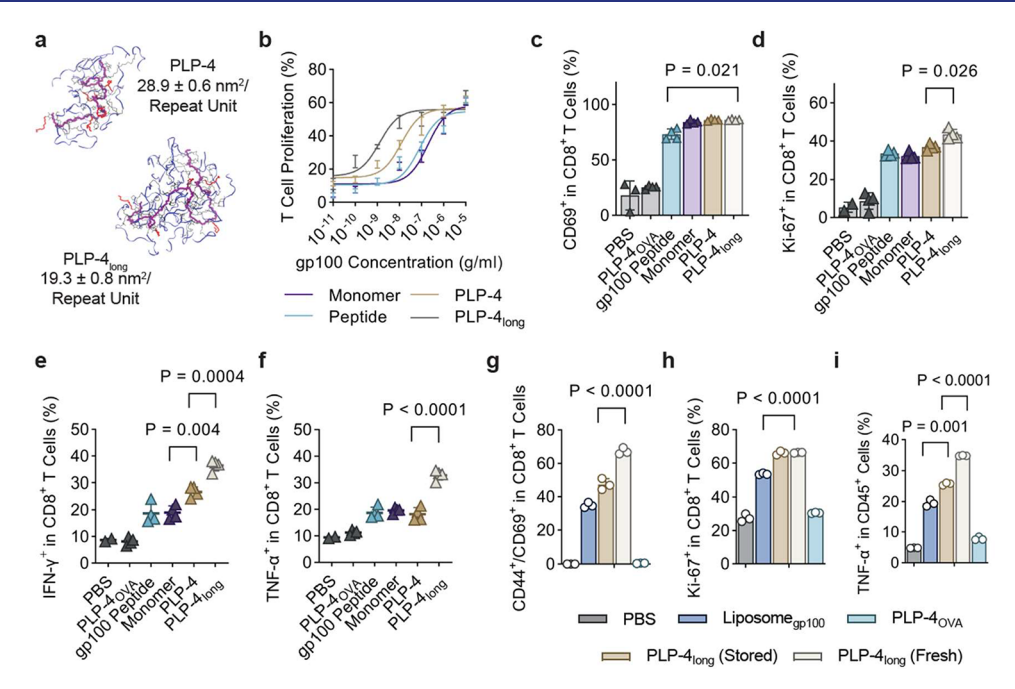


Figure 4. PLPs promote CD8⁺ T cell proliferation and activation in an antigen-specific and formulation dependent manner more efficiently than comparable liposomal formulations. (a) *in silico* models of short and long PLPs showing differences in globularity and antigen exposure quantified using SASA per repeat unit (n = 8 independent simulations) Purple: PLP backbone, Red: OEG side chains, Blue Ribbons: antigen side chains. (b) Dose—response curve of PLP treatment on CD8⁺ T cell proliferation following incubation for 72 h with Pmel-1 splenocytes. Three replicates are shown for each point. Curves show three-parameter dose—response fits. (c–f) Pmel-1 splenocytes were incubated with indicated treatments at a 1 μg/mL peptide concentration for 72 h. Percentages of Pmel-1 CD8⁺ T cells that were positive for CD69 (c) or expressed K_1 -67 (d) (n = 4 independent samples per group). Expression of IFN-γ (e) and TNF-α (f) in Pmel-1 CD8+ T cells following *ex vivo* restimulation was analyzed using flow cytometry (n = 4 independent samples per group). (g–i) Comparison of stored and freshly prepared PLPs to a liposomal formulation. Pmel-1 splenocytes were incubated with indicated treatments at a 10 μg/mL peptide concentration for 72 h. PLP-4_{long} (Stored) was stored as a lyophilized powder at -20 °C for >18 months. Expression of CD44/CD69 (g), K_1 -67 (h), and TNF-α (i) in CD8⁺ T cells as analyzed by flow cytometry (n = 3 independent samples per group). Data depict mean \pm s.d. *P*-values determined by one-way ANOVA throughout. Experiment repeated with similar results.

\$10). Computational and experimental studies on similar PLP structures have shown incorporation of a diluent amount of OEG can improve aqueous phase solubility. 12 PEGylation is also known to promote activation of APCs and cross-priming of CTLs. 23,33,34 As such, copolymer PLP formulations with norbornene-OEG4 monomers interspersed throughout were also tested (Figure S3 and Table S2) with uptake in splenic CD11b⁺/CD11c⁺ DCs quantified by FACS (Figure S11). A significant linkage and side chain composition trend was found, with PLP-4 having the highest fluorescence levels, followed by PLP-3 (Figure 2b, Figure S12). It was somewhat surprising that differential levels of uptake were observed between PLPs 1-3, which have conserved physical properties outside of linkage chemistry. However, these results are consistent with reports in other systems showing that reducible linkages result in higher levels of dendritic cell uptake, endosomal localization, and antigen cross-presentation. 35-37 We hypothesized that this observed difference in uptake could be partially explained by the increased endosomal retention of disulfide linked PLPs.

To examine subcellular localization, confocal microscopy was performed on PLP-treated BMDCs (Figure 2c,d), where a formulation-dependent trend emerged. Disulfide linkages displayed the highest levels of endosomal localization with PLP-4 maintaining the highest levels of endosomal entrapment (Figure S12). The increased uptake of disulfide containing PLPs and endosomal retention time of OEG-containing copolymers are consistent with trends seen in other nanoplatforms, ^{38–40} resulting in longer exposure to a reductive

environment expected to release disulfide-linked antigens for processing and cross presentation. 35,41,42 OEG-containing copolymers were also able to evoke higher levels of BMDC activation (Figure 2e) and, as such, were focused on going forward.

PLP Copolymers Induce BMDC-Mediated Antigen-Specific T Cell Priming *in Vitro* in a Linkage-Dependent Manner. The copolymers PLP-4, -5, and -6 were constructed with a 15:5 peptide:OEG ratio (Figure 1c) and characterized using SEC-MALS showing good agreement with theoretical values (Figure S3 and Table S2). Similar zeta potentials were measured for PLPs consisting of the same linkages with and without OEG (Figure 1d). PLP copolymers incubated with trypsin had reduced levels of proteolysis compared with homopolymers, maintaining the same established trend between linkages (Figure S8b).

Having shown favorable uptake profiles and cleavage kinetics, the ability of PLP-treated APCs to induce T cell priming was probed. BMDCs were pulsed with PLPs or free peptide prior to coincubation with gp100-specific CD8⁺ T cells from pmel-1 mice¹⁶ to track payload-specific immune activation⁴³ and DC primed CTL responses³² (Figure 3a). A linkage chemistry dependent difference in gp100-specific T cell proliferation was detected (Figure 3b, Figure S13), with both cleavable linkages boosting proliferation at all DC ratios tested. Of note, PLPs with antigen conjugated using a stable amide linkage performed better than the free antigen peptide at a stimulator-to-responder ratio of 1:8. Both CD69 and

CD44^{high}/CD62L^{high} expression showed PLP-4 and PLP-5 outperforming other treatment arms, with PLP-4 evoking the highest levels of activated and central memory T cells (Figure 3c,d, Figure S14). PLP-4 was also superior at stimulating the production of IFN- γ , TNF- α , and Granzyme B (Figure 3e-g, Figure S15). No significant difference in cell viability was seen between the groups (Figure S16).

To confirm PLP activity was antigen-specific, PLPs containing an unrelated OVA antigen (PLP-4_{OVA}, Table S1) were forged and compared to the gp100-containing PLP-4 (Figure 3h, Figure S17). PLP-4_{OVA} was able to induce more OVA-specific CD8+ T cell proliferation and cytokine production compared to free OVA peptides alone in its cognate OT-1 system. Notably, PLP-4 failed to provoke OT-1 T cell proliferation, validating the generalizability of the PLP platform to carry different antigen payloads to initiate antigenspecific immune responses. Having down selected the disulfide linkage copolymer as the lead candidate, formulations were further optimized by modulating DP.

Effects of Increasing DP on DC Activation. Both the dose and density of antigen used in vaccine formulations are known to affect the magnitude of the elicited immune response.44,45 Since PLP structures covalently link multiple side chains, increasing DP, or molecular weight, simultaneously increases both the amount and the density of antigens per uptake event. Longer length disulfide-containing PLPs (PLP-4_{long}) were fabricated and characterized (Figure 1, Figure S3, Table S2). PLPs with DPs greater than 35 had limited solubility and were not studied further. Cy5.5 labeled PLP-4 $_{\rm long}$ was efficiently internalized by BMDCs and colocalized in endosomes. Additionally, flow cytometry showed similar levels of polymer fluorescence between PLP-4_{long} and PLP-4 (Figure S12). However, since dosage was performed relative to Cy5.5 concentration (~one dye per polymer), the total amount of antigen delivered by PLP-4 $_{\mathrm{long}}$ was roughly double that of PLP-

In the absence of serum preincubation, PLP-3, PLP-4, and PLP- 4_{long} induced similar levels of BMDC activation, as measured by CD86 expression (Figure S9). However, PLP-4_{long} maintained higher levels of activation compared with lower DP PLPs following preincubation in serum, likely due to decreased degradation. To quantify the extent of degradation, trypsin cleavage rates were monitored via HPLC (Figure S8c). PLPs showed a decrease in proteolysis as DP increased and following the addition of OEG side chains. A series of all-atom explicit solvent molecular dynamics simulations were performed to closely examine these observed effects. For computational simplicity, exact DPs of either 15 or 30 peptide side chains with and without 5 OEG side chains (i.e., single molecular entities) were simulated (Figure S18, Table S3). Increasing DP resulted in increased overall globularity and density of antigen payloads as well as decreased average solvent accessible surface area (SASA) per side chain (Figure 4a), representing reduced exposure to the surrounding environment.²⁶ The trypsin cleavage site SASA was also determined using spherical probes with a radius of either 3.14 or 0.14 nm to mimic a protein or water molecule, respectively (Figure S19). Using a protein-sized probe, increasing DP led to decreased accessibility of the cleavage site irrespective of the chemical linkage or presence of OEG, consistent with experimental data. However, simulated PLPs with OEG did not show significant differences in SASA. This is partially explained by the limited duration and number of molecules

simulated, with copolymers showing large variations between independent simulations. Copolymer proteolytic resistance could also be independent of cleavage site SASA, but rather from hindered engagement with proteases. 46 Water-sized probes showed uniform levels of accessible surface areas across all constructs, suggesting that peptide side chains maintain accessibility to small molecules such as GSH.

As PLP treatment increased expression levels of CD86 in BMDCs (Figure S9), the mechanism behind these effects was examined by RNA sequencing. BMDCs were treated with either PLP-4_{long}, confirmed to be endotoxin free (Figure S20), or LPS, a quintessential innate immune activator, and transcriptomic features compared. Kyoto Encyclopedia of Genes and Genomes (KEGG) enrichment analysis showed 343 transcripts differentially expressed compared to LPS treatment, with most enriched genes being involved in antigen processing and presentation, innate immune responses, and inflammatory responses (Figure S21). Comparison of a select set of genes showed similar levels of enrichment in antigen processing and presentation pathways between PLP-4_{long} and LPS treated BMDCs. However, genes involved in NOD-like receptors and phagosomes were not as highly enriched following PLP- 4_{long} treatment compared to those following LPS. This differential transcriptomic profile suggests that these particular PLPs are capable of stimulating BMDC activation and antigen presentation, albeit to a mild extent.

Next, the ability of PLPs to cultivate antigen-specific T cell activity was examined. A disulfide monomer group was included to check for effects of the terminal free thiol remaining following bond reduction. A dose response curve tracking antigen-specific T cell proliferation following incubation of Pmel-1 splenocytes (which contain a mixture of both APCs and T cells) was generated (Figure 4b, Figure S22) showing proliferation saturating at 10 μ g/mL for all groups. However, at lower concentrations, DP has a significant effect on T cell proliferation with only PLP-4_{long} having detectable T cell proliferation at 100 pg/mL. No difference was detected between the free gp100 peptide and monomer treatments, suggesting minimal interference of the residual thiol group. Following a three day incubation at a lower 1 μ g/ mL concentration, pmel T cells treated with either PLP-4 or PLP-4_{long} both showed higher levels of CD69 (Figure 4c) and K_i-67 (Figure 4d, Figure S23) compared to free peptide or monomer. PLP-4_{long} treated pmel T cells showed significantly higher expression levels of IFN-γ (Figure 4e, Figure S23) and TNF- α (Figure 4f) compared to PLP-4 which was marginally higher than peptide/monomer treatment. PLP-4_{OVA} meanwhile was comparable to that of PBS, confirming antigenspecific effects.

PLPs Perform Better than Comparable Liposome Formulations and Can Be Stored Frozen. We next compared the optimized PLP formulation to the currently available liposome-based delivery platforms. One major limitation of liposomal formulations is their need to be manufactured at point of use or implementation of complex protocols and addition of cryoprotectants for long-term storage in a lyophilized state. 47-49 Comparatively, PLPs can be lyophilized, stored in the powder state for extended periods of time, and redispersed without loss in activity. Pmel-1 splenocytes were incubated with gp100 at the same peptide concentration either conjugated to a PLP or encapsulated within a liposome (See Supplemental Methods). CD8+ T cell activation and proliferation markers, as well as TNF- α

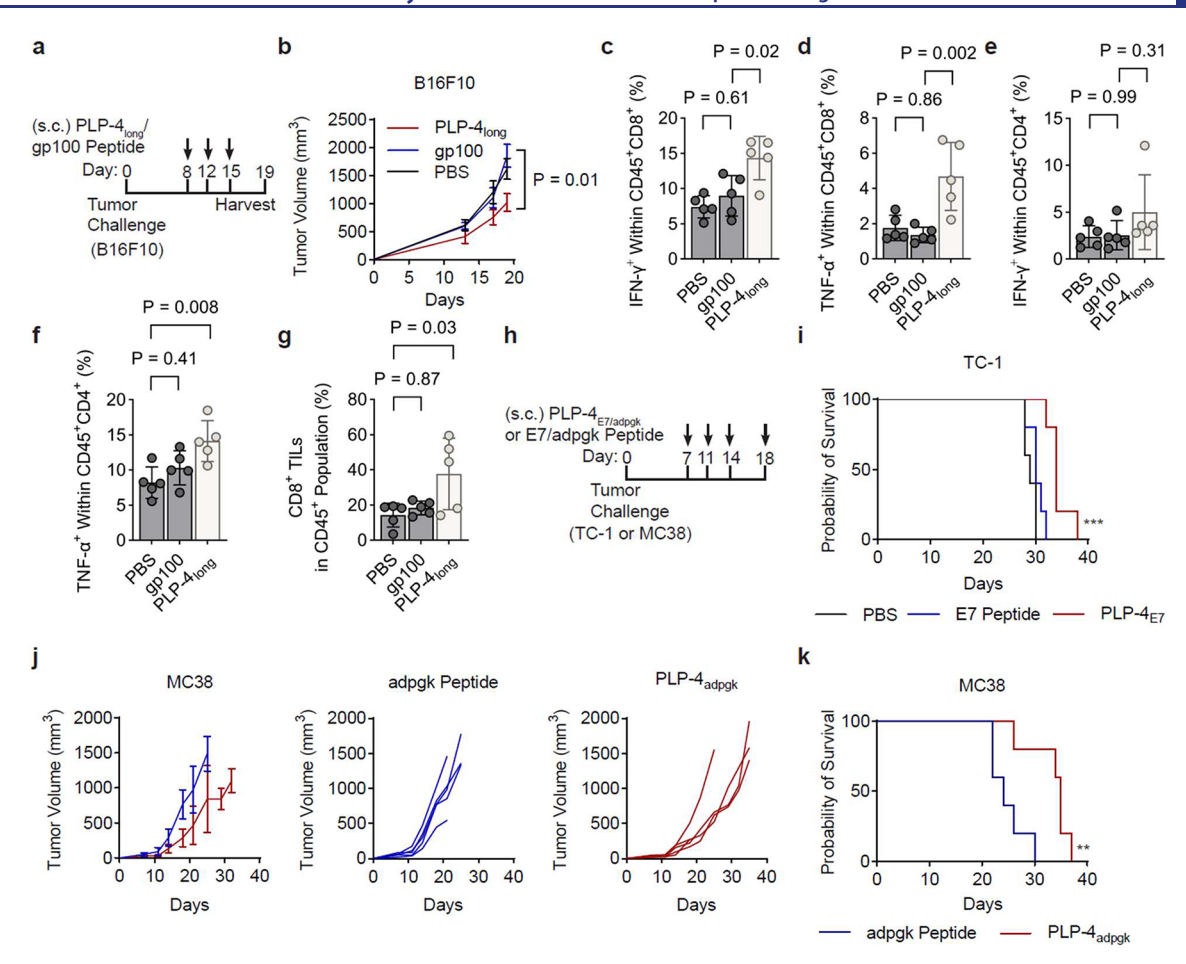


Figure 5. PLP vaccination suppressed tumor growth in three mouse tumor models. B16F10 tumor cells expressing gp100 (0.5 × 10⁶) were subcutaneously (s.c.) implanted in C57BL/6 mice and allowed to establish for 8 days until tumors were palpable. Treatment schedule (a) and tumor growth curves (b) of mice vaccinated three times s.c. with free peptide or PLP-4 (100 μ g gp100 dose) at days 8, 12, and 15 as indicated (n = 5 mice per group, compared with PBS). Tumors and dLNs were excised at day 19, stimulated *ex vivo* (see Supplemental Methods), and proportions of IFN- γ ⁺ and TNF- α ⁺ cells in CD45⁺/CD8⁺ (c,d) or CD45⁺/CD4⁺ (e,f) dLN populations or CD8⁺ TILs (g) were analyzed by flow cytometry (n = 5 mice per group). (h) Mice bearing TC-1 or MC38 tumors were injected subcutaneously with corresponding peptides or PLPs as monotherapy at indicated days post tumor challenge (100 μ g antigen per dose). (i–k) Survival and individual tumor growth curves. Data depict mean \pm s.d. P-values determined by one-way ANOVA at day 19 (b–g) or log-rank test (i,k). ***P < 0.001; **P < 0.01.

expression in CD45⁺ cells were significantly higher for both freshly prepared and PLPs stored lyophilized at -20 °C for >18 months compared to liposomes (Figure 4g-i). PLPs containing OVA side chains were used as payload controls, showing no immune cell activation, further confirming that raised immune responses are antigen-specific. Taken together, these results underscore the clinical relevance of PLPs as they can be fabricated in advance and stored until use.

PLPs Traffic to the Draining Lymph Node and Slow Tumor Growth in Multiple Tumor Models. Whether PLP vaccination can suppress tumor growth *in vivo* was next assessed in mice bearing established B16F10 melanoma tumors overexpressing gp100 and treated with gp100 carrying PLP-4_{long}. First, to confirm PLPs injected subcutaneously traffic to draining lymph nodes (dLN), tumor bearing mice were injected subcutaneously with one dose of Cy5.5-labeled PLPs and imaged after 3 h (Figure S24a). Twenty-four hours post injection, organs were excised and imaged *ex vivo* (Figure S24b,c). PLPs were shown to accumulate primarily in the tumor and dLN, with confocal laser-scanning microscopy confirming retention of fluorescent signal in the organ. Residual fluorescent signal was also detected in the liver,

kidney, and spleen, although how precisely PLPs are metabolized and excreted remain to be determined.

Next, the ability of PLPs to induce an immune response was examined. Vaccination with PLP-4_{long} alone resulted in significantly inhibited tumor growth compared to vehicle or peptide treatment (Figure 5a,b). Tumors and dLN were also excised, processed, and analyzed on day 19. Flow cytometry analysis of dLN cells following ex vivo stimulation (Supplemental Methods) showed increased IFN- γ and TNF- α expression in the general CD8+ (Figure 5c,d) and CD4+ (Figure 5e,f) T cell populations. In addition, the proportion of polyfunctional (IFN γ^+ TNF α^+) CD8⁺ and CD4⁺ T cells in the dLN is roughly double compared to that of PBS controls (Figure S25). PLP treatment also resulted in a significant increase in the proportion of CD8+ tumor infiltrating lymphocytes (TILs) (Figure 5g), K_i-67 expression, and CD44⁺/CD62L⁻ effector phenotype in these CD8⁺ TILs (Figure S26a,b). Frequency of CD4⁺ Foxp3⁺ regulatory T cell (T_{reg}) populations was lower in PLP treated tumors, and these T_{reg} expressed lower levels of K_i -67 (Figure S26c,d).

We employed two additional established tumor models to further probe the ability of the PLP platform to induce

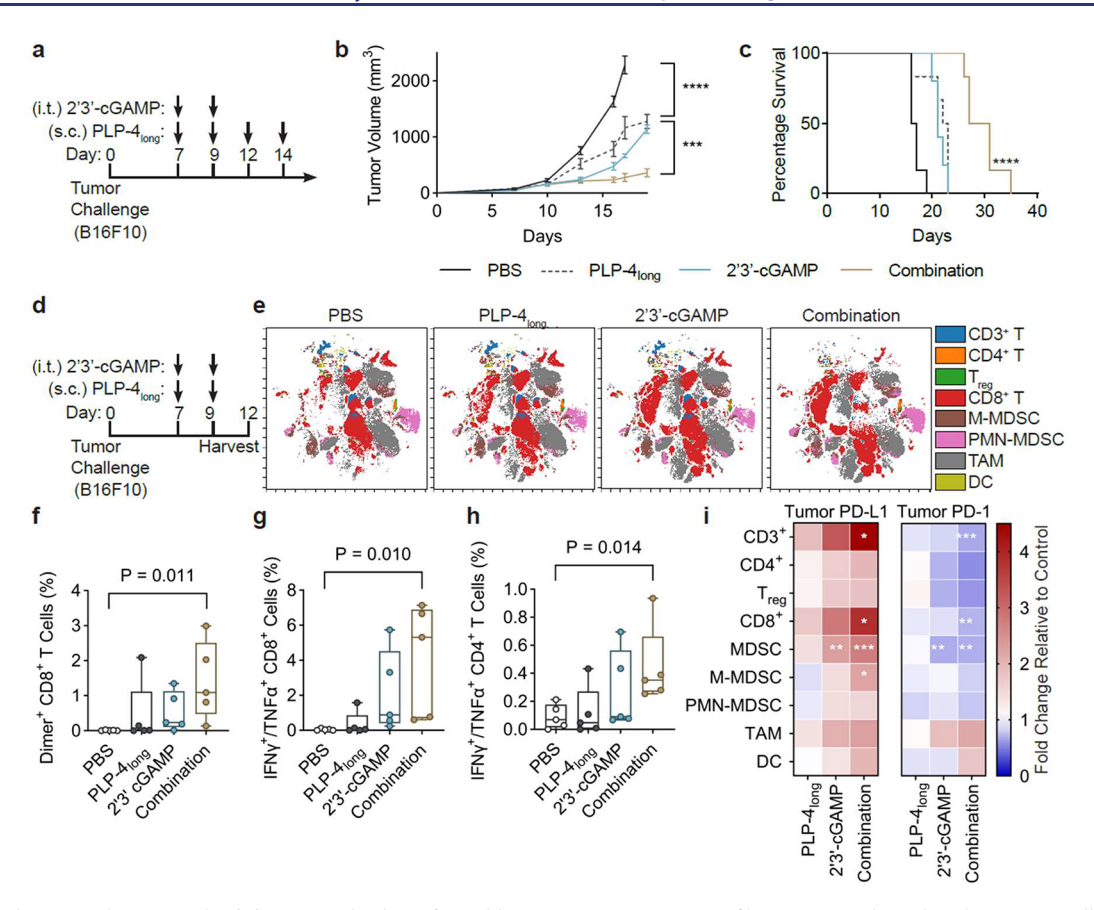


Figure 6. Combination therapy with 2'3'-cGAMP leads to favorable antitumor immune profiles. Mice implanted with B16F10 cells (0.5×10^6) allowed to establish a palpable tumor were treated with PLP-4_{long} (100 μg gp100, given s.c.) and STING agonist 2'3'-cGAMP (10 μg, given i.t.) alone or in combination. Experimental timeline (a), tumor growth curves (b), and overall survival (c) in C57BL/6 mice vaccinated with indicated treatments (n = 6 mice/group). (d) Experimental timeline of mice bearing established B16F10 tumors (allowed to develop for 8 days) given indicated treatments with tumors harvested at day 14 for analysis (n = 5 mice/group). (e) t-distributed stochastic neighbor embedding (t-SNE) visualization of tumor-infiltrating leukocytes across different treatment groups. Percentages of gp100-specific TILs in the total tumor cell population, determined by gp100 dimer staining (f), and total tumor cells that are polyfunctional (IFN-γ+ TNF-α+) CD8+ (g) or CD4+ (h) following *ex vivo* restimulation. (i) Fold changes in mean fluorescence intensity of PD-L1 and PD-1 relative to PBS treated control cohort in excised tumor samples stratified by cell type and treatment group (significant differences vs PBS control noted). Data depict mean ± s.d. *P*-values were determined by log-rank test (c) or one-way ANOVA (f-h). ****P < 0.0001; ***P < 0.001; **P < 0.01; *P < 0.05.

payload-specific antitumor immunity, a human papillomavirusassociated TC-1 model⁵⁰ and a high mutational burden MC38 colon carcinoma model.⁵¹ Briefly, PLPs were synthesized with either E7⁴⁻⁷ (PLP-4_{E7}) or adpgk⁵² (PLP-4_{adpgk}) peptide antigens as the payload, all formulated as the lead configuration (PLP-4_{long}) consisting of roughly 30 antigen side chains conjugated to the polymer backbone via a disulfide linkage and copolymerized with OEG₄ (Figure S27). C57BL/6 mice were inoculated subcutaneously with either TC-1 or MC38 cells, tumors were allowed to establish, and immunized twice weekly with PLP-4_{E7} or PLP-4_{adpgk} as monotherapies, respectively (Figure 5h), with survival compared to mice treated with either unpolymerized free peptide or vehicle control (Figure 5i-k). Dosage was again performed relative to the amount of peptide antigen at 100 μ g/dose, a concentration when administered as a free peptide is indistinguishable from vehicle treatment. Significant extensions in survival were conferred following immunization with PLPs alone in both tumor lines compared to control and peptide treatment arms (median survival in days: TC-1, PBS = 29, PLP- 4_{E7} = 35; MC38, PBS = 24, PLP- $4_{adpgk} = 35$). These results highlight the generalizability of the PLP platform, including ability to deliver anionic sequences to suppress tumor growth as single agent therapies.

PLP Vaccination Acts Synergistically with STING Agonists. Given the conserved ability of PLPs to induce antigen-specific T cell responses in vivo, paired with transcription-level information on the pathways upregulated following monotherapy, we predicted complementary combination treatment with agonists for the STING pathway, a crucial innate immune component for establishing neoantigenspecific T cell priming,14 would increase vaccine efficacy and regress established tumors. 5,6-dimethylxanthenone-4-acetic acid (DMXAA), a STING ligand previously shown effective in multiple mouse models^{53–55} was initially tested. Vaccination with PLP-4_{long} paired with DMXAA resulted in impressively suppressed tumor growth compared with treatment with either agent alone (Figure S28). A PLP-4 plus DMXAA combination therapy arm was also included, which was shown to not be as effective as the PLP-4_{long} combination therapy, verifying trends seen in vitro.

With promising results following combination therapy with DMXAA, we next tested combination therapy with a clinically relevant, STING agonist, 2'3'-cGAMP.⁵⁶⁻⁵⁸ Mice bearing B16F10 melanoma were treated with gp100-carrying PLPs and/or 2'3'-cGAMP (Figure 6a). 2'3'-cGAMP was given intratumorally due to its poor pharmacokinetic profiles and

rapid degradation by hydrolases, necessitating local administration for activity. $^{59-61}$ Combination therapy resulted in the highest inhibition of tumor growth and median survival times, with 50% surviving over 30 days post tumor implantation (Figure 6b,c). Strikingly, treatment with PLP-4_{long} alone was indistinguishable from 2'3'-cGAMP monotherapy on survival times. Direct comparison to combination therapy with free peptide plus 2'3-cGAMP confirmed the superior efficacy of PLP-4_{long} over vaccination with free peptide when given in conjunction with the small molecule STING agonist (Figure S29).

To assess the quality of the immune response induced by PLP vaccination, mice were treated with a short two treatment regimen of PLP-4_{long} and/or 2'3'cGAMP (Figure 6d), again showing combination therapy significantly inhibits tumor growth (Figure S30). On day 14, the tumor and spleens were excised and analyzed using spectrum cytometry (Cytek) (Figure S31). We used the dimensionality reduction tool viSNE to differentiate treatment-induced antitumor immune effects. Live CD45⁺ tumor infiltrates could be clearly grouped into distinct major immune cell subsets, and a CD8+ T cell cluster tended to be enriched on the viSNE map following treatment with PLP-4_{long} or 2'3'-cGAMP (Figure 6e). Closer examination showed minor changes in immune cell type frequency between treatment groups in both the tumor and spleen, with slightly elevated proportions of CTLs in tumors and Tumor-associated macrophages (TAMs) in spleens of mice treated with combination therapy and lower levels of MDSCs (Figure S32). However, tumor-infiltrating CD8⁺ and CD4⁺ T cells (TILs) in mice treated with combination PLP and 2'3'-cGAMP showed significantly higher levels of gp100specific TILs (Figure 6f) and polyfunctional IFN- γ^+ TNF- α^+ CD8+ and CD4+ T cells (Figure 6g,h) following ex vivo restimulation with mildly elevated single-expression of IFN- γ^+ or TNF- α^+ (Figure S33). CD3⁺ cells, CD8⁺ T cells, and MDSCs in the tumor of animals treated with combination therapy showed significantly higher levels of PD-L1 and decreased levels of PD-1 compared to vehicle treated controls with mild changes following 2'3'-cGAMP monotherapy (Figure 6i). Splenocytes also showed mild increases in PD-1 expression in T_{reo}, CD8⁺ T cells, MDSCs, and TAMs (Figure \$34). The lower MDSC population, increased proportion of cytokine producing lymphocytes, and reduced TIL exhaustion profile together suggest combination treatment improves T cell quality in the tumor, explaining the observed differences in disease progression.

Finally, to confirm generalizability of the observed treatment synergy with 2'3-cGAMP to a second tumor model, mice bearing TC-1 tumors were treated with combination therapy of PLP-4_{E7} plus 2'3'-cGAMP as well as each treatment alone (Figure 7a). Again, combination therapy showed the highest levels of tumor suppression, with ~40% of mice in the treatment group being tumor-free at 60 days post challenge (Figure 7b). These tumor-free mice were subsequently rechallenged on day 60 with a second inoculation of fresh TC-1 cells in the opposite flank, without additional treatments and followed over time. Of these rechallenged mice, all rejected the newly implanted TC-1 cells, compared to a naive reference group, which were not previously immunized (Figure 7c). These results suggest that strong immunological memory was generated by combination therapy of PLP-4_{E7} plus 2'3'cGAMP which led to long-term tumor protection. To screen for toxic effects resulting from PLP treatment, healthy mice

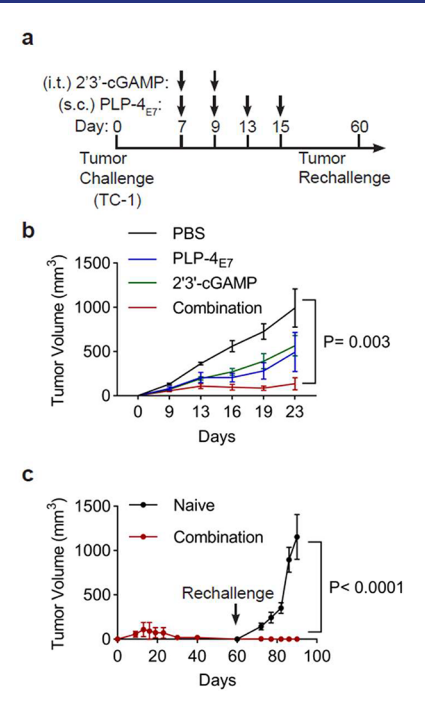


Figure 7. PLP vaccination synergizes with 2'3'-cGAMP to induce sustained antitumor effects. (a) Experimental timeline of TC-1 tumorbearing mice treated with PBS, PLP-4_{E7}, 2'3'-cGAMP, or the combination of the two as indicated. (b) Tumor growth curves for each treatment arm (n = 7 mice/group). (c) Lasting immunological memory was assessed in mice treated with the combination therapy that rejected initial TC-1 tumor implantation and were tumor-free until day 60 and were subsequently rechallenged with a second inoculation of TC-1 cells. Naive mice were used as controls. Data depict mean ± s.d. P-values were determined by one-way ANOVA (b) or Student's *t* test (c).

were injected with high doses of PLPs and body weight was monitored (Figure S35) showing no changes.

CONCLUSION

Extensive research has been devoted to the development of strategies that coopt the immune system to treat and, in certain cases, eradicate cancers. Despite this, clinical translation has remained limited, particularly in cancer vaccine development. This can partially be attributed to several interrelated barriers, including poor lymph node trafficking, low APC uptake, and suboptimal antigen immunogenicity. Here, we describe the novel PLP platform, which allows for the facile cultivation of potent immunotherapies that conveniently can be stored and frozen for extended periods of time. Several advantageous properties emerge when peptides are arranged as PLPs, stemming from the graft-through polymerization method used in their synthesis, wherein monomers are directly functionalized with peptides prior to polymerization, resulting in dense brush polymers with every side chain occupied by a peptide sequence. Previous studies have used graft-to methods, coupling peptide antigens to a functionalized backbone chain to forge low-density polymers. 62,63 Compared to graft-through PLPs, graft-to polymers exhibit modest grafting efficiencies due to steric bulk and charge repulsion leading to batch to batch variations.⁶⁴ Additionally, PLPs as described here use a hydrophobic peptide norbornylimide monomer conferring resistance to proteolytic degradation as the polymers collapse

to form globular structures via hydrophobic effects, while providing for efficient cell penetration and uptake.²⁰

Using a library of PLP formulations with conserved antigenic side chains but varied physical parameters, we demonstrate that the PLP structure plays a determining role in raising cellular immune responses and antitumor outcomes following immunotherapy. How peptide antigens are conjugated onto a PLP backbone (cleavable vs noncleavable), the specific composition of polymer side chains (with or without OEG), and the density of display (long vs short) all were found to influence the final elicited immune reaction. The differing immunostimulatory effects observed between PLP formulations is a consequence of distinct uptake and subcellular trafficking profiles in DCs, paired with variations in proteolytic stability, the sum of which ultimately determines the quality of effector cell function and antigen-specific killing of tumor cells in vivo.

The findings of this study, which utilized a structure-based approach, highlight both the tunability of the PLP platform and how slight modifications in chemical design can lead to dramatically disparate immune outcomes. While previous studies on vaccine design have demonstrated the importance of structure-function relationships as it pertains to raised immune responses following vaccination, 7,20,65-67 PLPs are particularly well suited for this application as their construction permits a wide range of chemical modification while allowing precise sequence-level control over side chains. This enables both the chemical tuning of immune activation and the manufacturing of polymers with limited molecule-to-molecule and batch-to-batch variation. Building on this technology, this study aimed to establish preliminary design rules governing the immunogenicity of antigen carrying PLPs. To achieve this, we employed a series of optimization steps to downselect PLP- 4_{long} as the lead candidate for *in vivo* assessment.

Key parameters that were found to impact payload-specific immune activation include inclusion of a disulfide linkage reducible by APCs allowing for loading onto MHC molecules, incorporation of the OEG to increase proteolytic stability and endosomal entrapment, and increasing the DP to improve retention and quantity of internalized antigen per uptake event. Interestingly, PLPs with cleavable disulfide linkages were found to evoke mild DC activation on their own. Although the key mechanisms underlying this activity warrant further study, transcriptomic analysis revealed that PLP treatment enhances pathways involved in antigen processing and presentation.

In a direct comparison between our compounds to currently available platforms, both newly synthesized PLPs and ones stored frozen for >18 months performed better than liposomes at the same antigen dose, spotlighting the unique advantages of the PLP platform and its ease of use. Single agent treatments with PLPs resulted in marked increases in survival times in three different tumor models, further confirming the generalizability of the platform. Additionally, vaccination in an aggressive melanoma model given in conjunction with STING agonists resulted in increased antitumor CD8+ T cell responses, leading to an improved survival and tumor control. Tumor and spleen analysis of PLP-treated mice showed elevated expression of PD-L1 and PD-1 across cell types, which is known to be upregulated following STING activation. 68,69 As dysregulation of the B7-H1/PD-1 pathway is a common immune evasion mechanism in the tumor microenvironment, addition of checkpoint inhibitors may be a viable adjunct therapy to augment PLP vaccine response. Although this study

was limited in the scope of tumor peptide antigens explored, the overall approach is generalizable to any individual peptide sequence, as well as combinations of sequences. The insights on PLP design derived from this work lay the foundation for the facile assembly of complex personalized vaccine formulations based on this platform with potential ramifications for the treatment of cancer and other diseases.

EXPERIMENTAL SECTION

Experimental details can be found in the accompanying Supporting Information file.

ASSOCIATED CONTENT

Supporting Information

The Supporting Information is available free of charge at https://pubs.acs.org/doi/10.1021/jacs.3c05340.

Detailed material syntheses and characterizations, experimental details, HPLC spectra, mass spectra, ¹H NMR spectra, SEC-MALS traces, additional confocal microscopy images, flow cytometry gating strategies and representative dot plots, All-atom MD simulation parameters, and RNaseq results (PDF)

AUTHOR INFORMATION

Corresponding Authors

Bin Zhang - Robert H. Lurie Comprehensive Cancer Center, Department of Medicine-Division of Hematology/Oncology, Northwestern University Feinberg School of Medicine, Chicago, Illinois 60611, United States; o orcid.org/0000-0002-6631-7647; Email: bin.zhang@northwestern.edu

Nathan C. Gianneschi – Department of Chemistry, Department of Biomedical Engineering, International Institute for Nanotechnology, Simpson Querrey Institute, Chemistry of Life Processes Institute, Robert H. Lurie Comprehensive Cancer Center, and Department of Materials Science and Engineering, Northwestern University, Evanston, Illinois 60208, United States; Department of Pharmacology, Northwestern University Feinberg School of Medicine, Chicago, Illinois 60208, United States; oorcid.org/0000-0001-9945-5475; Email: nathan.gianneschi@ northwestern.edu

Authors

Max M. Wang - Department of Chemistry, Department of Biomedical Engineering, and International Institute for Nanotechnology, Simpson Querrey Institute, Chemistry of Life Processes Institute, Robert H. Lurie Comprehensive Cancer Center, Northwestern University, Evanston, Illinois 60208, United States; orcid.org/0000-0002-2810-8561

Mi-Ran Choi - Robert H. Lurie Comprehensive Cancer Center, Department of Medicine-Division of Hematology/ Oncology, Northwestern University Feinberg School of Medicine, Chicago, Illinois 60611, United States

Claudia Battistella - Department of Chemistry and International Institute for Nanotechnology, Simpson Querrey Institute, Chemistry of Life Processes Institute, Robert H. Lurie Comprehensive Cancer Center, Northwestern University, Evanston, Illinois 60208, United States

Brayley Gattis - Department of Chemistry and International Institute for Nanotechnology, Simpson Querrey Institute, Chemistry of Life Processes Institute, Robert H. Lurie

- Comprehensive Cancer Center, Northwestern University, Evanston, Illinois 60208, United States
- Baofu Qiao Department of Materials Science and Engineering, Northwestern University, Evanston, Illinois 60208, United States; Department of Natural Sciences, Baruch College, City University of New York, New York, New York 10010, United States; orcid.org/0000-0001-8870-5985
- Michael Evangelopoulos Department of Biomedical Engineering and International Institute for Nanotechnology, Simpson Querrey Institute, Chemistry of Life Processes Institute, Robert H. Lurie Comprehensive Cancer Center, Northwestern University, Evanston, Illinois 60208, United States; orcid.org/0000-0002-5300-4289
- Chad A. Mirkin Department of Chemistry, Department of Biomedical Engineering, International Institute for Nanotechnology, Simpson Querrey Institute, Chemistry of Life Processes Institute, Robert H. Lurie Comprehensive Cancer Center, and Department of Materials Science and Engineering, Northwestern University, Evanston, Illinois 60208, United States; orcid.org/0000-0002-6634-7627
- Monica Olvera de la Cruz Department of Chemistry and Department of Materials Science and Engineering, Northwestern University, Evanston, Illinois 60208, United States; orcid.org/0000-0002-9802-3627

Complete contact information is available at: https://pubs.acs.org/10.1021/jacs.3c05340

Author Contributions

*M.M.W. and M.-R.C. contributed equally. C.B., B.Z., and N.C.G. conceived of and planned the project. C.B., B.Z., and N.C.G. set the goals and determined the deliverables. C.B. trained M.M.W. on lab methods. M.M.W. prepared polymeric materials together with B.G. with initial input from C.B. M.-R.C. performed *in vivo* studies together with M.M.W. with the initial aid of C.B. B.Q. performed all simulations under the supervision of M.O.C., providing all analyses of the *in silico* results together with N.C.G. and M.M.W. M.E. prepared vesicle controls under the supervision of C.A.M. M.M.W. led the drafting of the manuscript, produced figures, and analyzed results together with M.-R.C., B.Z., and N.C.G. All authors discussed the results and edited the manuscript.

Notes

The authors declare the following competing financial interest(s): N.C.G. is a co-founder of Grove Biopharma, which is a licensee of intellectual property (IP) related to the science and materials found in this manuscript. N.C.G., C.B., M.M.W., and B.Z. are co-inventors on that same IP.

ACKNOWLEDGMENTS

We would like to thank M. Thompson for providing peptide resins, D. Dominguez for assistance with cell culture, the veterinary staff at the Center for Comparative Medicine, the Immunotherapy Assessment Core Facility, and the RHLCCC Flow Cytometry Core Facility. This work made use of the IMSERC MS and NMR facilities at Northwestern University, which has received support from the Soft and Hybrid Nanotechnology Experimental (SHyNE) Resource (NSF ECCS-2025633), Int. Institute of Nanotechnology, and Northwestern University. This work was made possible by the support of the NIH through R01CA222963 and R01CA257926, as well as the National Science Foundation

through DMR-2004899. This work was also partially funded by a Sherman Fairchild Innovation Challenge Award from the Lurie Cancer Center. M.M.W. was supported by SF30CA257519-02. B.G. was supported by NSF-GRFP No. DGE-1842165. M.E. was supported by the Alexander S. Onassis Public Benefit Foundation.

REFERENCES

- (1) Waldman, A. D.; Fritz, J. M.; Lenardo, M. J. A guide to cancer immunotherapy: from T cell basic science to clinical practice. *Nature Reviews Immunology* **2020**, *20* (11), 651–668.
- (2) Irvine, D. J.; Dane, E. L. Enhancing cancer immunotherapy with nanomedicine. *Nature Reviews Immunology* **2020**, 20 (5), 321–334.
- (3) Khalil, D. N.; Smith, E. L.; Brentjens, R. J.; Wolchok, J. D. The future of cancer treatment: immunomodulation, CARs and combination immunotherapy. *Nature Reviews Clinical Oncology* **2016**, *13* (5), 273–290.
- (4) Krishnamachari, Y.; Geary, S. M.; Lemke, C. D.; Salem, A. K. Nanoparticle delivery systems in cancer vaccines. *Pharm. Res.* **2011**, 28 (2), 215–236.
- (5) Kuai, R.; Ochyl, L. J.; Bahjat, K. S.; Schwendeman, A.; Moon, J. J. Designer vaccine nanodiscs for personalized cancer immunotherapy. *Nat. Mater.* **2017**, *16* (4), 489–496.
- (6) Li, A. W.; Sobral, M. C.; Badrinath, S.; Choi, Y.; Graveline, A.; Stafford, A. G.; Weaver, J. C.; Dellacherie, M. O.; Shih, T.-Y.; Ali, O. A.; et al. A facile approach to enhance antigen response for personalized cancer vaccination. *Nat. Mater.* **2018**, *17* (6), 528–534.
- (7) Wang, S.; Qin, L.; Yamankurt, G.; Skakuj, K.; Huang, Z.; Chen, P.-C.; Dominguez, D.; Lee, A.; Zhang, B.; Mirkin, C. A. Rational vaccinology with spherical nucleic acids. *Proc. Natl. Acad. Sci. U. S. A.* **2019**, *116* (21), 10473.
- (8) Carreno, B. M.; Magrini, V.; Becker-Hapak, M.; Kaabinejadian, S.; Hundal, J.; Petti, A. A.; Ly, A.; Lie, W. R.; Hildebrand, W. H.; Mardis, E. R.; et al. Cancer immunotherapy. A dendritic cell vaccine increases the breadth and diversity of melanoma neoantigen-specific T cells. *Science* **2015**, *348* (6236), 803–808.
- (9) Ott, P. A.; Hu, Z.; Keskin, D. B.; Shukla, S. A.; Sun, J.; Bozym, D. J.; Zhang, W.; Luoma, A.; Giobbie-Hurder, A.; Peter, L.; et al. An immunogenic personal neoantigen vaccine for patients with melanoma. *Nature* **2017**, *547* (7662), 217–221.
- (10) Keskin, D. B.; Anandappa, A. J.; Sun, J.; Tirosh, I.; Mathewson, N. D.; Li, S.; Oliveira, G.; Giobbie-Hurder, A.; Felt, K.; Gjini, E.; et al. Neoantigen vaccine generates intratumoral T cell responses in phase Ib glioblastoma trial. *Nature* **2019**, *565* (7738), 234–239.
- (11) Bachmann, M. F.; Jennings, G. T. Vaccine delivery: a matter of size, geometry, kinetics and molecular patterns. *Nature Reviews Immunology* **2010**, *10* (11), 787–796.
- (12) Blum, A. P.; Kammeyer, J. K.; Yin, J.; Crystal, D. T.; Rush, A. M.; Gilson, M. K.; Gianneschi, N. C. Peptides Displayed as High Density Brush Polymers Resist Proteolysis and Retain Bioactivity. *J. Am. Chem. Soc.* **2014**, *136* (43), 15422–15437.
- (13) Callmann, C. E.; Thompson, M. P.; Gianneschi, N. C. Poly(peptide): Synthesis, Structure, and Function of Peptide—Polymer Amphiphiles and Protein-like Polymers. *Acc. Chem. Res.* **2020**, 53 (2), 400–413.
- (14) Motwani, M.; Pesiridis, S.; Fitzgerald, K. A. DNA sensing by the cGAS-STING pathway in health and disease. *Nat. Rev. Genet.* **2019**, 20 (11), 657–674.
- (15) Marincola, F. M.; Hijazi, Y. M.; Fetsch, P.; Salgaller, M. L.; Rivoltini, L.; Cormier, J.; Simonis, T. B.; Duray, P. H.; Herlyn, M.; Kawakami, Y.; et al. Analysis of expression of the melanoma-associated antigens MART-1 and gp100 in metastatic melanoma cell lines and in in situ lesions. *J. Immunother Emphasis Tumor Immunol* 1996, 19 (3), 192–205.
- (16) Overwijk, W. W.; Tsung, A.; Irvine, K. R.; Parkhurst, M. R.; Goletz, T. J.; Tsung, K.; Carroll, M. W.; Liu, C.; Moss, B.; Rosenberg, S. A.; et al. gp100/pmel 17 is a murine tumor rejection antigen:

- induction of "self"-reactive, tumoricidal T cells using high-affinity, altered peptide ligand. J. Exp Med. 1998, 188 (2), 277–286.
- (17) Kammeyer, J. K.; Blum, A. P.; Adamiak, L.; Hahn, M. E.; Gianneschi, N. C. Polymerization of Protecting-Group-Free Peptides via ROMP. *Polym. Chem.* **2013**, *4*, 3929–3933.
- (18) Dong, H.; Pang, L.; Cong, H.; Shen, Y.; Yu, B. Application and design of esterase-responsive nanoparticles for cancer therapy. *Drug Deliv* **2019**, 26 (1), 416–432.
- (19) Collins, D. S.; Unanue, E. R.; Harding, C. V. Reduction of disulfide bonds within lysosomes is a key step in antigen processing. *J. Immunol* **1991**, *147* (12), 4054–4059.
- (20) Skakuj, K.; Wang, S.; Qin, L.; Lee, A.; Zhang, B.; Mirkin, C. A. Conjugation Chemistry-Dependent T-Cell Activation with Spherical Nucleic Acids. *J. Am. Chem. Soc.* **2018**, *140* (4), 1227–1230.
- (21) Hirosue, S.; Kourtis, I. C.; van der Vlies, A. J.; Hubbell, J. A.; Swartz, M. A. Antigen delivery to dendritic cells by poly(propylene sulfide) nanoparticles with disulfide conjugated peptides: Cross-presentation and T cell activation. *Vaccine* **2010**, 28 (50), 7897–7906.
- (22) van der Vlies, A. J.; O'Neil, C. P.; Hasegawa, U.; Hammond, N.; Hubbell, J. A. Synthesis of Pyridyl Disulfide-Functionalized Nanoparticles for Conjugating Thiol-Containing Small Molecules, Peptides, and Proteins. *Bioconjugate Chem.* **2010**, 21 (4), 653–662.
- (23) Nam, J.; Son, S.; Park, K. S.; Moon, J. J. Modularly Programmable Nanoparticle Vaccine Based on Polyethyleneimine for Personalized Cancer Immunotherapy. *Advanced Science* **2021**, 8 (5), No. 2002577.
- (24) Hoshyar, N.; Gray, S.; Han, H.; Bao, G. The effect of nanoparticle size on in vivo pharmacokinetics and cellular interaction. *Nanomedicine (Lond)* **2016**, *11* (6), 673–692.
- (25) He, C.; Hu, Y.; Yin, L.; Tang, C.; Yin, C. Effects of particle size and surface charge on cellular uptake and biodistribution of polymeric nanoparticles. *Biomaterials* **2010**, *31* (13), 3657–3666.
- (26) Sun, H.; Qiao, B.; Choi, W.; Hampu, N.; McCallum, N. C.; Thompson, M. P.; Oktawiec, J.; Weigand, S.; Ebrahim, O. M.; de la Cruz, M. O.; et al. Origin of Proteolytic Stability of Peptide-Brush Polymers as Globular Proteomimetics. *ACS Central Science* **2021**, 7 (12), 2063–2072.
- (27) Meister, A. Glutathione metabolism and its selective modification. J. Biol. Chem. 1988, 263 (33), 17205-17208.
- (28) Jones, D. P.; Carlson, J. L.; Samiec, P. S.; Sternberg, P., Jr.; Mody, V. C., Jr.; Reed, R. L.; Brown, L. A. Glutathione measurement in human plasma. Evaluation of sample collection, storage and derivatization conditions for analysis of dansyl derivatives by HPLC. Clin. Chim. Acta 1998, 275 (2), 175–184.
- (29) Artigas, J. M.; Garcia, M. E.; Faure, M. R.; Gimeno, A. M. Serum trypsin levels in acute pancreatic and non-pancreatic abdominal conditions. *Postgrad Med. J.* **1981**, *57* (666), 219–222.
- (30) Porgador, A.; Snyder, D.; Gilboa, E. Induction of antitumor immunity using bone marrow-generated dendritic cells. *J. Immunol.* **1996**, *156* (8), 2918.
- (31) Paglia, P.; Chiodoni, C.; Rodolfo, M.; Colombo, M. P. Murine dendritic cells loaded in vitro with soluble protein prime cytotoxic T lymphocytes against tumor antigen in vivo. *J. Exp Med.* **1996**, *183* (1), 317–322.
- (32) Celluzzi, C. M.; Mayordomo, J. I.; Storkus, W. J.; Lotze, M. T.; Falo, L. D., Jr. Peptide-pulsed dendritic cells induce antigen-specific CTL-mediated protective tumor immunity. *J. Exp Med.* **1996**, *183* (1), 283–287.
- (33) Vllasaliu, D.; Fowler, R.; Stolnik, S. PEGylated nanomedicines: recent progress and remaining concerns. *Expert Opinion on Drug Delivery* **2014**, *11* (1), 139–154.
- (34) Turecek, P. L.; Bossard, M. J.; Schoetens, F.; Ivens, I. A. PEGylation of Biopharmaceuticals: A Review of Chemistry and Nonclinical Safety Information of Approved Drugs. *J. Pharm. Sci.* **2016**, *105* (2), 460–475.
- (35) Hirosue, S.; Kourtis, I. C.; van der Vlies, A. J.; Hubbell, J. A.; Swartz, M. A. Antigen delivery to dendritic cells by poly(propylene sulfide) nanoparticles with disulfide conjugated peptides: Crosspresentation and T cell activation. *Vaccine* **2010**, 28 (50), 7897–7906.

- (36) Li, P.; Luo, Z.; Liu, P.; Gao, N.; Zhang, Y.; Pan, H.; Liu, L.; Wang, C.; Cai, L.; Ma, Y. Bioreducible alginate-poly(ethylenimine) nanogels as an antigen-delivery system robustly enhance vaccine-elicited humoral and cellular immune responses. *J. Controlled Release* **2013**, *168* (3), 271–279.
- (37) Slütter, B.; Soema, P. C.; Ding, Z.; Verheul, R.; Hennink, W.; Jiskoot, W. Conjugation of ovalbumin to trimethyl chitosan improves immunogenicity of the antigen. *J. Controlled Release* **2010**, *143* (2), 207–214.
- (38) Mishra, S.; Webster, P.; Davis, M. E. PEGylation significantly affects cellular uptake and intracellular trafficking of non-viral gene delivery particles. *European Journal of Cell Biology* **2004**, 83 (3), 97–111.
- (39) Suk, J. S.; Xu, Q.; Kim, N.; Hanes, J.; Ensign, L. M. PEGylation as a strategy for improving nanoparticle-based drug and gene delivery. *Adv. Drug Delivery Rev.* **2016**, *99*, 28–51.
- (40) Zhang, R.; Qin, X.; Kong, F.; Chen, P.; Pan, G. Improving cellular uptake of therapeutic entities through interaction with components of cell membrane. *Drug Deliv* **2019**, *26* (1), 328–342.
- (41) Hastings, K. T.; Cresswell, P. Disulfide reduction in the endocytic pathway: immunological functions of gamma-interferon-inducible lysosomal thiol reductase. *Antioxid Redox Signal* **2011**, *15* (3), 657–668.
- (42) van der Vlies, A. J.; O'Neil, C. P.; Hasegawa, U.; Hammond, N.; Hubbell, J. A. Synthesis of pyridyl disulfide-functionalized nanoparticles for conjugating thiol-containing small molecules, peptides, and proteins. *Bioconjug Chem.* **2010**, 21 (4), 653–662.
- (43) Labeur, M. S.; Roters, B.; Pers, B.; Mehling, A.; Luger, T. A.; Schwarz, T.; Grabbe, S. Generation of tumor immunity by bone marrow-derived dendritic cells correlates with dendritic cell maturation stage. *J. Immunol* 1999, 162 (1), 168–175.
- (44) Bullock, T. N. J.; Colella, T. A.; Engelhard, V. H. The Density of Peptides Displayed by Dendritic Cells Affects Immune Responses to Human Tyrosinase and gp100 in HLA-A2 Transgenic Mice. *J. Immunol.* 2000, 164 (5), 2354.
- (45) Kapadia, C. H.; Tian, S.; Perry, J. L.; Luft, J. C.; DeSimone, J. M. Role of Linker Length and Antigen Density in Nanoparticle Peptide Vaccine. ACS Omega 2019, 4 (3), 5547–5555.
- (46) Harris, J. M.; Chess, R. B. Effect of pegylation on pharmaceuticals. *Nat. Rev. Drug Discovery* **2003**, 2 (3), 214–221.
- (47) Franzé, S.; Selmin, F.; Samaritani, E.; Minghetti, P.; Cilurzo, F. Lyophilization of Liposomal Formulations: Still Necessary, Still Challenging. *Pharmaceutics* **2018**, *10* (3), 139.
- (48) Anchordoquy, T. J.; Koe, G. S. Physical stability of nonviral plasmid-based therapeutics. *J. Pharm. Sci.* **2000**, *89* (3), 289–296.
- (49) Zhao, P.; Hou, X.; Yan, J.; Du, S.; Xue, Y.; Li, W.; Xiang, G.; Dong, Y. Long-term storage of lipid-like nanoparticles for mRNA delivery. *Bioact Mater.* **2020**, *5* (2), 358–363.
- (50) Lin, K. Y.; Guarnieri, F. G.; Staveley-O'Carroll, K. F.; Levitsky, H. I.; August, J. T.; Pardoll, D. M.; Wu, T. C. Treatment of established tumors with a novel vaccine that enhances major histocompatibility class II presentation of tumor antigen. *Cancer Res.* 1996, 56 (1), 21–26.
- (51) Hos, B. J.; Camps, M. G. M.; van den Bulk, J.; Tondini, E.; van den Ende, T. C.; Ruano, D.; Franken, K.; Janssen, G. M. C.; Ru, A.; Filippov, D. V.; et al. Identification of a neo-epitope dominating endogenous CD8 T cell responses to MC-38 colorectal cancer. *Oncoimmunology* **2020**, *9* (1), No. 1673125.
- (52) Teplensky, M. H.; Evangelopoulos, M.; Dittmar, J. W.; Forsyth, C. M.; Sinegra, A. J.; Wang, S.; Mirkin, C. A. Multi-antigen spherical nucleic acid cancer vaccines. *Nat. Biomed. Eng.* **2023**, *7*, 911.
- (53) Weiss, J. M.; Guérin, M. V.; Regnier, F.; Renault, G.; Galy-Fauroux, I.; Vimeux, L.; Feuillet, V.; Peranzoni, E.; Thoreau, M.; Trautmann, A.; et al. The STING agonist DMXAA triggers a cooperation between T lymphocytes and myeloid cells that leads to tumor regression. *Oncoimmunology* **2017**, *6* (10), No. e1346765.
- (54) Jing, W.; McAllister, D.; Vonderhaar, E. P.; Palen, K.; Riese, M. J.; Gershan, J.; Johnson, B. D.; Dwinell, M. B. STING agonist inflames the pancreatic cancer immune microenvironment and reduces tumor

- burden in mouse models. Journal for ImmunoTherapy of Cancer 2019, 7 (1), 115.
- (55) Corrales, L.; Glickman, L. H.; McWhirter, S. M.; Kanne, D. B.; Sivick, K. E.; Katibah, G. E.; Woo, S. R.; Lemmens, E.; Banda, T.; Leong, J. J.; et al. Direct Activation of STING in the Tumor Microenvironment Leads to Potent and Systemic Tumor Regression and Immunity. *Cell Rep* **2015**, *11* (7), 1018–1030.
- (56) Conlon, J.; Burdette, D. L.; Sharma, S.; Bhat, N.; Thompson, M.; Jiang, Z.; Rathinam, V. A.; Monks, B.; Jin, T.; Xiao, T. S.; et al. Mouse, but not human STING, binds and signals in response to the vascular disrupting agent 5,6-dimethylxanthenone-4-acetic acid. *J. Immunol* 2013, 190 (10), 5216–5225.
- (57) Gutjahr, A.; Papagno, L.; Nicoli, F.; Kanuma, T.; Kuse, N.; Cabral-Piccin, M. P.; Rochereau, N.; Gostick, E.; Lioux, T.; Perouzel, E. The STING ligand cGAMP potentiates the efficacy of vaccine-induced CD8+ T cells. *JCI Insight* **2019**, DOI: 10.1172/jci.insight.125107.
- (58) Kinkead, H. L.; Hopkins, A.; Lutz, E.; Wu, A. A.; Yarchoan, M.; Cruz, K.; Woolman, S.; Vithayathil, T.; Glickman, L. H.; Ndubaku, C. O. Combining STING-based neoantigen-targeted vaccine with checkpoint modulators enhances antitumor immunity in murine pancreatic cancer. *JCI Insight* 2018, DOI: 10.1172/jci.insight.122857.
- (59) Demaria, O.; De Gassart, A.; Coso, S.; Gestermann, N.; Di Domizio, J.; Flatz, L.; Gaide, O.; Michielin, O.; Hwu, P.; Petrova, T. V.; et al. STING activation of tumor endothelial cells initiates spontaneous and therapeutic antitumor immunity. *Proc. Natl. Acad. Sci. U. S. A.* **2015**, *112* (50), 15408–15413.
- (60) Petrovic, M.; Borchard, G.; Jordan, O. Considerations for the delivery of STING ligands in cancer immunotherapy. *J. Controlled Release* **2021**, 339, 235–247.
- (61) Ohkuri, T.; Kosaka, A.; Ishibashi, K.; Kumai, T.; Hirata, Y.; Ohara, K.; Nagato, T.; Oikawa, K.; Aoki, N.; Harabuchi, Y.; et al. Intratumoral administration of cGAMP transiently accumulates potent macrophages for anti-tumor immunity at a mouse tumor site. Cancer Immunology, Immunotherapy 2017, 66 (6), 705–716.
- (62) Bennett, N. R.; Zwick, D. B.; Courtney, A. H.; Kiessling, L. L. Multivalent Antigens for Promoting B and T Cell Activation. *ACS Chem. Biol.* **2015**, *10* (8), 1817–1824.
- (63) Bennett, N. R.; Jarvis, C. M.; Alam, M. M.; Zwick, D. B.; Olson, J. M.; Nguyen, H. V. T.; Johnson, J. A.; Cook, M. E.; Kiessling, L. L. Modular Polymer Antigens To Optimize Immunity. *Biomacromolecules* **2019**, 20 (12), 4370–4379.
- (64) Choi, W.; Sun, H.; Battistella, C.; Berger, O.; Vratsanos, M. A.; Wang, M. M.; Gianneschi, N. C. Biomolecular Densely Grafted Brush Polymers: Oligonucleotides, Oligosaccharides and Oligopeptides. *Angew. Chem., Int. Ed. Engl.* **2020**, *59* (45), 19762–19772.
- (65) Huang, Z.; Callmann, C. E.; Wang, S.; Vasher, M. K.; Evangelopoulos, M.; Petrosko, S. H.; Mirkin, C. A. Rational Vaccinology: Harnessing Nanoscale Chemical Design for Cancer Immunotherapy. ACS Cent Sci. 2022, 8 (6), 692–704.
- (66) Teplensky, M. H.; Dittmar, J. W.; Qin, L.; Wang, S.; Evangelopoulos, M.; Zhang, B.; Mirkin, C. A. Spherical Nucleic Acid Vaccine Structure Markedly Influences Adaptive Immune Responses of Clinically Utilized Prostate Cancer Targets. *Adv. Healthcare Mater.* **2021**, *10* (22), No. e2101262.
- (67) Skakuj, K.; Teplensky, M. H.; Wang, S.; Dittmar, J. W.; Mirkin, C. A. Chemically Tuning the Antigen Release Kinetics from Spherical Nucleic Acids Maximizes Immune Stimulation. *ACS Cent Sci.* **2021**, 7 (11), 1838–1846.
- (68) Moore, E.; Clavijo, P. E.; Davis, R.; Cash, H.; Van Waes, C.; Kim, Y.; Allen, C. Established T Cell-Inflamed Tumors Rejected after Adaptive Resistance Was Reversed by Combination STING Activation and PD-1 Pathway Blockade. *Cancer Immunol Res.* **2016**, 4 (12), 1061–1071.
- (69) Fu, J.; Kanne, D. B.; Leong, M.; Glickman, L. H.; McWhirter, S. M.; Lemmens, E.; Mechette, K.; Leong, J. J.; Lauer, P.; Liu, W.; et al. STING agonist formulated cancer vaccines can cure established tumors resistant to PD-1 blockade. *Sci. Transl Med.* **2015**, 7 (283), No. 283ra252.

(70) Dong, H.; Strome, S. E.; Salomao, D. R.; Tamura, H.; Hirano, F.; Flies, D. B.; Roche, P. C.; Lu, J.; Zhu, G.; Tamada, K.; et al. Tumor-associated B7-H1 promotes T-cell apoptosis: a potential mechanism of immune evasion. *Nat. Med.* **2002**, *8* (8), 793–800.